Dalton Transactions

PAPER

View Article Online
View Journal

Cite this: DOI: 10.1039/c8dt04229b

Crowding out: ligand modifications and their structure directing effects on brucite-like $\{M_x(\mu_3\text{-OH})_y\}$ (M = Co(II), Ni(II)) core growth within polymetallic cages†

Mari E. Slater-Parry,[a] James P. Durrant,[a] Joshua M. Howells,[a] Mateusz B. Pitak,[b] Peter N. Horton,[b] Wim T. Klooster,[b] Simon J. Coles,[b] Helen M. O'Connor,[c] Euan K. Brechin,[c] Anne-Laure Barra[d] and Leigh F. Jones *[a]

Received 23rd October 2018,
Accepted 20th December 2018

DOI: 10.1039/c8dt04229b

rsc.li/dalton

Previous employment of the ligands 2-methoxy-6-[(methylimino)methyl]phenol (L_1H) and 2-methoxy-6-[(phenylimino)methyl]phenol (L_2H) has resulted in the self-assembly of pseudo metallocalix[6]arene complexes of general formulae: $[M_7(\mu_3\text{-OH})_6(L_x)_6](NO_3)_y$ (M = Ni(II), x = 1, y = 2 (**1**) and Co(II/III), x = 2, y = 3 (**2**)). Extrapolating upon this work, we report the coordination chemistry of ligands 2-methoxy-6-{[(2-methoxyphenyl)imino]methyl}phenol (L_3H), 2-[(benzylimino)methyl]-6-methoxyphenol (L_4H), 2-[(benzylamino)methyl]-6-methoxyphenol (L_5H) and 2-[(benzylamino)methyl]-4-bromo-6-methoxyphenol (L_6H), whose structures are modifications of ligands $L_{1-2}H$. These ligands are employed in the synthesis and characterisation of the dimetallic complex $[Ni(II)_2(L_3)_3(H_2O)](NO_3)\cdot 2H_2O\cdot 3MeOH$ (**3**); the monometallic complexes $[Ni(II)(L_4)_2]$ (**4**) and $[Co(III)(L_4)_3]\cdot H_2O\cdot MeOH$ (**5a**); and the tetranuclear pseudo metallocalix[4]arene complexes: $[(NO_3)\subset Co(II)_4(\mu_3\text{-OH})_2(L_5)_4(H_2O)_2](NO_3)\cdot H_2O$ (**6**), $[(NO_3)\subset Ni(II)_4(\mu_3\text{-OH})_2(L_5)_4(H_2O)_2](NO_3)\cdot H_2O$ (**7**) and $[Ni(II)_4(\mu_3\text{-OH})_2(L_6)_4(NO_3)_2]\cdot MeCN$ (**8**). The tetrametallic 'butterfly' core topologies in **6–8** are discussed with respect to their structural and topological relationship with their heptanuclear $[M_7]$ (M = Co(II), Ni(II)) pseudo metallocalix[6]arene ancestors (**1** and **2**).

Introduction

The ligands 2-methoxy-6-[(methylimino)methyl]phenol (L_1H) and 2-methoxy-6-[(phenylimino)methyl]phenol (L_2H; Scheme 1) have previously been employed for the formation of the pseudo metallocalix[6]arene complexes $[M_7(\mu_3\text{-OH})_6(L_x)_6](NO_3)_y$ (M = Ni(II), x = 1, y = 2 (**1**) and Co(II/III) x = 2, y = 3 (**2**)) (Fig. 1).[1] Each of these compounds exhibit a double-bowl topology and in the solid state form molecular cavities that are able to act as hosts for guests such as small organics and counter anions.[1] The heptanuclear inorganic cores in **1** and **2** are best described as comprising six edge-sharing triangular $\{M_3(\mu_3\text{-OH})\}$ (M = Ni(II)/Co(II/III)) units, resulting in planar sheet-like, body-centred hexagonal arrays (Fig. 1), whereby each octahedral metal centre is connected by μ_3-bridging OH^- ions. Similar sheet-like $\{M_x(\mu_3\text{-OH})_y\}$ topologies have been reported for a variety of transition metal cages of numerous nuclearities, such as $[M_4]$ (M = Mn,[2] Fe,[3] Co,[4] Ni[5] and Zn[6]), $[Ni_5]$,[7] $[Ni_6]$,[8] $[M_7]$ (M = Mn,[9,13] Fe,[10] Co,[1c,11] Ni[1a,b,12] and Zn[1b,13]), $[Mn_{10}]$,[14] $[Co_{12}]$,[15] $[Fe_{17}]$,[16] $[Ni_{18}]$,[17] $[M_{19}]$ (M = Mn,[18] Fe[16]) and $[Co_{28}]$.[15] ‡

Moreover, the observation of such planar 'Single Layer Double Hydroxide' (SLDH) topologies is not surprising when we consider their similarities to the sheet-like brucite ('Layered Double Hydroxides'; LDH) topologies observed in minerals such as the α- and β-polymorphs of $Co(OH)_2$ [19] and $Ni(OH)_2$,[20] as well as the familiar brucite structure of $Mg(OH)_2$. Interestingly, cobalt and nickel hydroxides hold significant interest in the field of water splitting catalysis. More specifically, in 2008 Nocera and co-workers devised an efficient Co $(OH)_2$/phosphate (Co-OEC) oxygen-evolving catalyst produced

[a]School of Natural Sciences, Bangor University, Bangor, Wales, LL57 2DG, UK. E-mail: leigh.jones@bangor.ac.uk; Tel: +44(0)1248-38-2391
[b]UK National Crystallographic Service, Chemistry, Faculty of Natural and Environmental Sciences, University of Southampton, England SO17 1BJ, UK
[c]EaStCHEM School of Chemistry, David Brewster Road, University of Edinburgh, Edinburgh, Scotland, EH9 3FJ, UK
[d]LNCMI-CNRS, Universite Grenoble-Alpes, Avenue des Martyrs, Grenoble, France

†Electronic supplementary information (ESI) available. CCDC 1874840–1874846. For ESI and crystallographic data in CIF or other electronic format see DOI: 10.1039/c8dt04229b

‡CSD searches were limited to planar $M_x(\mu_3\text{-OH})_y$ double hydroxide layered sheets and any planar complexes with $M_x(\mu_3\text{-OR})_y$ cores (where OR = aryloxide or alkoxide) were omitted.

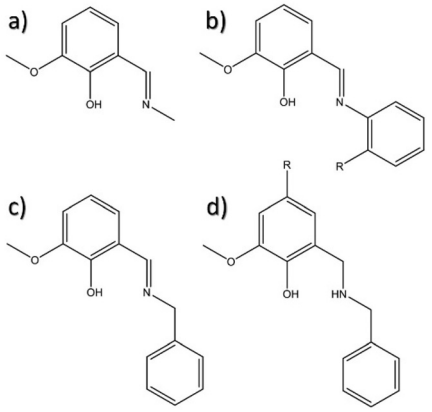

Scheme 1 ChemDraw representation of the ligands 2-methoxy-6-[(methylimino)methyl]phenol (L_1H; a) and 2-methoxy-6-[(phenylimino)methyl]phenol (in b when R = H; L_2H), used previously in the formation of $[M_7]$ (M = Co(II/III), Ni(II), Zn(II)) pseudo metallocalix[6]arenes (see main text for details). ChemDraw representations of the ligands 2-methoxy-6-{[(2-methoxyphenyl)imino]methyl}phenol (in b when R = OMe; L_3H), 2-[(benzylimino)methyl]-6-methoxyphenol (L_4H; c), 2-[(benzylamino)methyl]-6-methoxyphenol (in d where R = H; L_5H) and 2-[(benzylamino)methyl]-4-bromo-6-methoxyphenol (in d where R = Br; L_6H).

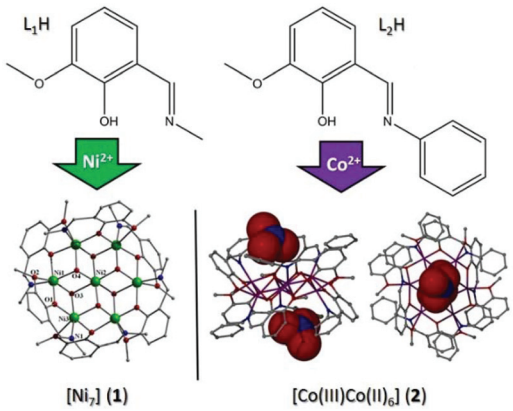

Fig. 1 Schematic depicting the coordination chemistry of ligands L_1H and L_2H upon reaction with Ni(II) and Co(II/III) ions. Single crystal X-ray data was used to produce the $[Ni_7]$ (**1**) and $[Co(III)Co(II)_6]$ (**2**) figures.[1] Colour code (used throughout this work): green (Ni), purple (Co), red (O), blue (N), grey (C). Hydrogen atoms omitted for clarity and NO_3^- counter anions represented in space-fill mode.

through electrode surface deposition that has been shown to exhibit topological similarities with the sheet-like structures in (for instance) β-$Co(OH)_2$ and many $M_x(\mu_3\text{-}OH)_y$ transition metal cages (*vide supra*).[21] It should also be noted here that $Ni(OH)_2$-borate thin film electrocatalysts have recently been produced by the same research group.[22] Interestingly, and to emphasise these similarities, the triflate analogues of our previously described homo- and heterovalent pseudo metallocalix[6]arenes $[Co(II)_7(\mu_3\text{-}OH)_6(L_1)_6](NO_3)_2$ and $[(NO_3)\subset Co(II)_6Co(III)(\mu_3\text{-}OH)_6(L_2)_6](NO_3)_2$ (**2**),[1c] respectively, were employed by Nocera and co-workers as models towards investigating the electron transfer kinetics of their cobalt-phosphate (Co-OEC) water splitting catalyst.[23]

Our aim in this work was to strategically modify the shape and electronic nature of the $[M_7]$ metallocalix[6]arene-directing ligands $L_{1-2}H$ (Scheme 1) and monitor any changes in resultant complex nuclearity and topology (*e.g.* $\{M_x(OH)_y\}$ sheet size) upon subsequent Co(II) and Ni(II) complexation. To this end, we report here the successful synthesis of the novel ligands 2-methoxy-6-{[(2-methoxyphenyl)imino]methyl}phenol (L_3H), 2-[(benzylimino)methyl]-6-methoxyphenol (L_4H), 2-[(benzylamino)methyl]-6-methoxyphenol (L_5H) and 2-[(benzylamino)methyl]-4-bromo-6-methoxyphenol (L_6H) (Scheme 1). We also present the first examples of transition metal complexation of ligands $L_{3-6}H$ in the form of complexes: $[Ni(II)(L_3)(H_2O)](NO_3)\cdot 2H_2O\cdot 3MeOH$ (**3**), $[Ni(II)(L_4)_2]$ (**4**) and $[Co(III)(L_4)_3]\cdot H_2O\cdot MeOH$ (**5a**), along with the tetranuclear compounds: $[(NO_3)\subset Co(II)_4(\mu_3\text{-}OH)_2(L_5)_4(H_2O)_2](NO_3)\cdot H_2O$ (**6**), $[(NO_3)\subset Ni(II)_4(\mu_3\text{-}OH)_2(L_5)_4](NO_3)\cdot H_2O$ (**7**) and $[Ni(II)_4(\mu_3\text{-}OH)_2(L_6)_4(NO_3)_2]\cdot$ MeCN (**8**). Crystallographic data for complexes **3–8** are given in Tables S1 and S2.†

Results and discussion

We began our investigations by looking at the complexation of 2-methoxy-6-(((2-methoxyphenyl)imino)methyl)phenol (L_3H) and Ni(II), which gives rise to the dimetallic complex $[Ni(II)_2(L_3)_3(H_2O)](NO_3)\cdot 2H_2O\cdot 3MeOH$ (**3**) and crystallises in the monoclinic $P2_1/n$ space group (Fig. 2). The two Ni(II) ions (Ni1 and Ni2) are bridged by phenolic oxygens (O1 and O5) of two L_3^- ligands exhibiting $\eta^1{:}\eta^2{:}\eta^1{:}\eta^1$ μ- and $\eta^2{:}\eta^1$ μ-bridging motifs, to give the angles 101.86° (Ni1–O1–Ni2) and 96.10°

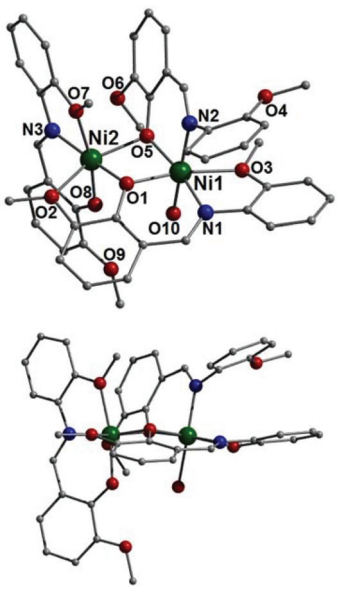

Fig. 2 Crystal structure of $[Ni(II)(L_3)(H_2O)](NO_3)\cdot 2H_2O\cdot 3MeOH$ (**3**) as viewed off-set and parallel to the Ni–O_{phen}–Ni plane. Hydrogen atoms and counter anions have been omitted for clarity.

(Ni1–O5–Ni2), respectively. The third L_3^- unit sits at approximately right angles to the Ni1–$O1_{phen}$–Ni2 plane and chelates (tridentate) at the Ni2 centre to complete its distorted octahedral geometry. The η^2:η^1 μ-bridging ligand in **3** has a much more contorted shape than the remaining two near planar L_3^- ligands, with its two aromatic rings twisted away from one another through rotation of the N_{imine}–C_{arom} (N2–C22) single bond to give a torsion angle (C23–N2–C22–C21) of 118.67° (Fig. 2). Interestingly, this twisting is also observed in all six L_2^- ligands used in constructing the pseudo metallocalix[6]arene $[(NO_3)\subset Co(II)_6Co(III)(\mu_3\text{-}OH)_6(L_2)_6](NO_3)_2$ (**2**) (Fig. 1). The introduction of the OMe group in L_3H, along with the fact that the remaining two L_3^- ligands in **3** remain almost planar plays a decisive role in the resultant dimeric topology. The final coordination site at Ni2 is taken by a single terminally bonded H_2O ligand (Ni1–O10 = 2.072(4) Å), whose protons partake in intramolecular H-bonding interactions with juxtaposed ligand O_{phen} (O10(H10A)···O8 = 2.02 Å) and OMe (O10(H10A)···O9 = 2.47 Å) oxygen donor atoms. The NO_3^- counter anions (N4, O18–O20) in **3** act as molecular mortar in connecting the individual $\{Ni(II)_2\}$ units through extensive H-bonding with aromatic protons of neighbouring bridging L_3^- ligands (C40(H40)···O18 = 2.58 Å, C36(H36)···O19 = 2.54 Å and C34(H34)···O20 = 2.42 Å). These dimeric units in **3** arrange in the common brickwork motif along the *bc* plane of the unit cell, with the 2D sheets packing in superimposable rows along the *a* unit cell direction (Fig. S4†).

The monometallic complex $[Ni(II)(L_4)_2]$ (**4**) crystallises from methanol in the triclinic $P\bar{1}$ space group (Z = 1) after reaction of $Ni(NO_3)_2{\cdot}6H_2O$ and L_4H in the presence of NaOH. The core in **4** comprises a single Ni(II) centre (labelled Ni1 and lying on an inversion centre) whose near perfect square planar geometry (N1–Ni1–N1 = 180°; O1–Ni1–N1′ = 87.46° and O1–Ni1–N1 = 92.54°) is templated by two chelating L_4^- ligands through their O_{phen} (O1) and imine N atoms (N1) (Fig. 3). This topology is vastly different to the heptanuclear cores in **1**–**2** (Fig. 1 *cf.* Fig. 3) and is attributed to the introduced methylene bridge between the imine and lower rim phenyl group in L_4H. Upon chelation the OMe and benzyl imine groups in the symmetry related L_4^- moieties in **4** significantly deviate from the plane of their phenolic rings, resulting in N1–C7–C6 and C13–O2–C15 angles of 111.11° and 112.45°, respectively (Fig. 3). Numerous intermolecular interactions stabilise and direct the topology in **4**. More specifically, the two symmetry equivalent L_4^- ligands are involved in intramolecular H-bonding as shown as dashed lines in Fig. 3 (O1···H7B′(C7′) = 2.19 Å, O2···(H5′(C5′) = 2.34 Å and the long contact: O2···H7B′(C7′) = 2.91 Å). Intermolecular H-bonding interactions between O atoms (O2 of the non-bonded –OMe group on L_4^-) and neighbouring aromatic protons (H5) effectively link the $\{Ni_1\}$ units into superimposable H-bonded rows along the *c* direction of the unit cell (O2···(H4′)C4′ = 2.65 Å) (Fig. S5†).

Reaction of L_4H with $Co(II)(NO_3)_2{\cdot}6H_2O$ gives rise to the co-crystallisation of the monometallic complex $[Co(III)(L_4)_3]{\cdot}H_2O{\cdot}MeOH$ (**5a**; purple needle-like crystals and predominant product), along with a much smaller quantity of red hexagonal crystals which were found to be the complex $[Co(II)_7(OMe)_6(L_4)_6](NO_3)_2{\cdot}0.5H_2O{\cdot}4MeOH$ (**5b**); whose structure is akin to the pseudo metallocalix[6]arenes of **1** and **2** (*cf.* Fig. 1 and Fig. 5). Interestingly, from a synthetic view point, the deliberate oxidation of Co(II) using hydrogen peroxide efficiently promotes the sole crystallisation of $[Co(III)(L_4)_3]{\cdot}H_2O{\cdot}MeOH$ (**5a**), over the formation of $[Co(II)_7(OMe)_6(L_4)_6](NO_3)_2{\cdot}0.5H_2O{\cdot}4MeOH$ (**5b**) (see Experimental section for details). However, despite numerous attempts using various reducing agents, our efforts in producing only **5b** were unsuccessful.

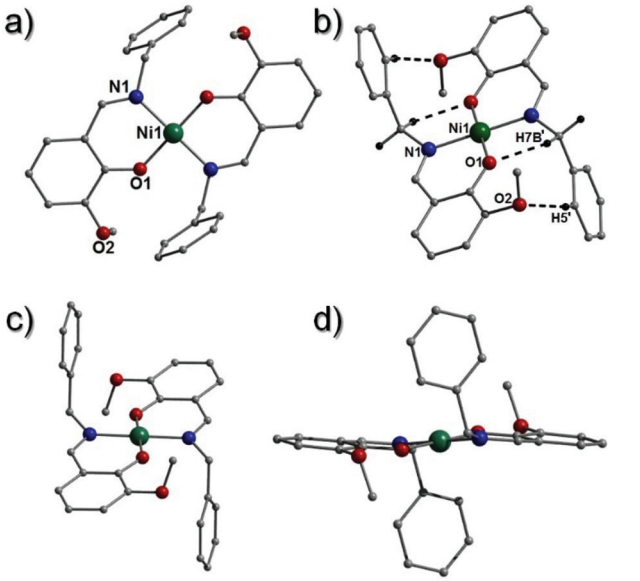

Fig. 3 Crystal structure of $[Ni(II)(L_4)_2]$ (**4**) as viewed perpendicular (a–c) and parallel (d) to the equatorial plane. Majority of hydrogen atoms have been omitted for clarity. Dashed lines are intramolecular H-bonds at distances: O1···H7B′(C7′) = 2.19 Å and O2···H5′(C5′) = 2.34 Å. The additional ′ symbol in the atom labels indicates that these atoms are at equivalent positions (1 – *x*, 1 – *y*, 1 – *z*).

The single Co(III) centre in **5a** (Bond Valence Sum (BVS) score = 3.22; Table S3†) is enveloped by three singly deprotonated L_4^- ligands that chelate the metal centre through their N_{imine} and O_{phen} atoms (bond length range: 1.882(2)–1.961(2) Å; Fig. 4). As observed in $[Ni(II)(L_4)_2]$ (**4**), the L_4^- phenyl groups in **5a** diverge from the plane of their phenolic rings to produce angles of 111.83° (N1–C9–C10), 113.60° (N2–C39–C40) and 112.80° (N3–C24–C25), along with torsion angles of 87.77° (C8–N1–C9–C10), 46.26° (C38–N2–C39–C40) and 97.47° (C23–N3–C24–C25) (Fig. 4).

$[Co(II)_7(OMe)_6(L_4)_6](NO_3)_2{\cdot}0.5H_2O{\cdot}4MeOH$ (**5b**) crystallises in the monoclinic $P2_1/c$ space group and there are two 'half' $\{Co(II)_7\}$ units in the asymmetric unit (labelled Co1–Co4 and Co5–Co8, respectively; centres Co1 and Co5 lie on inversion centres). The inorganic core in **5b** exhibits a planar body centred hexagonal array of Co(II) ions linked together with a combination of μ_3-bridging $^-$OMe and $^-$OH ions (50 : 50 occupancy; see Crystallography section for details). The Co(II) oxi-

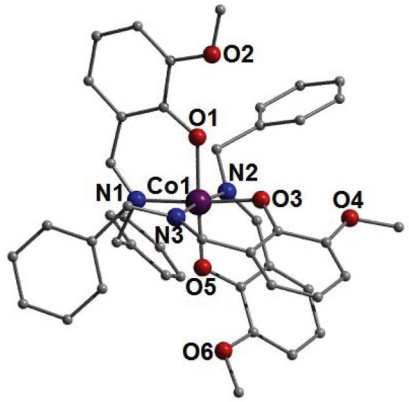

Fig. 4 Crystal structure of $[Co(III)(L_4)_3]\cdot MeOH\cdot H_2O$ (**5a**). Hydrogen atoms have been omitted for clarity.

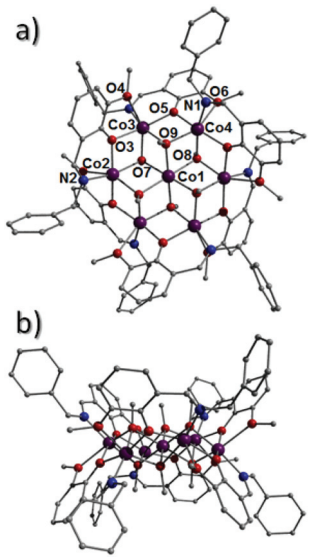

Fig. 5 Crystal structure observed in $[Co(II)_7(OMe)_6(L_4)_6](NO_3)_2\cdot H_2O\cdot 3MeOH$ (**5b**) as viewed perpendicular (a) and parallel (b) to the $\{Co(II)_7\}$ plane. Hydrogen atoms have been omitted for clarity.

dation states were assigned using BVS and charge balancing considerations. The outer Co(II) ions (Co2–Co4 and Co6–Co8, respectively) are further connected through $\eta^1{:}\eta^2{:}\eta^1$ μ-bridging L_4^- ligands that lie alternately above and below the planar $\{Co(II)_7\}$ core in **5b**, thus forming the double-bowl pseudo metallocalix[6]arene as observed in our previous studies (complexes **1** and **2**; Fig. 1). As with complexes **4** and **5a**, the phenyl ligand groups in **5b** twist away from their corresponding O_{phen} aromatic rings. Interestingly, the torsion angles produced in **5b** vary much more widely when compared with complexes **4** and **5a**, with values including 5.69° (C23–N2–C24–C25), 21.56° (C56–N4–C57–C58) and 89.19° (C86–N6–C87–C89). Thus the ligand conformational flexibility in L_4H, governed by free rotation along the N_{imine}–CH_2 bond, allows the feasible construction of both low (**4** and **5a**) and high nuclearity complexes (**5b**). The individual $[Co(II)_7]$ units arrange in superimposable rows along the *a* unit cell direction and pack along the *bc* plane in the space-efficient brickwork motif (Fig. S7†).

We speculated that by reducing the imine (C=N) bond in L_4H (to give ligand L_5H) we could manipulate ligand shape and allow multiple metal centre coordination and growth of a more complex inorganic core. This proved to be the case when Co(II)/Ni(II) metalation of L_5H (and L_6H) gave rise to the tetranuclear complexes: $[(NO_3)\subset Co(II)_4(\mu_3\text{-}OH)_2(L_5)_4(H_2O)_2](NO_3)\cdot H_2O$ (**6**), $[(NO_3)\subset Ni(II)_4(\mu_3\text{-}OH)_2(L_5)_4(H_2O)_2](NO_3)\cdot H_2O$ (**7**) and $[Ni(II)_4(\mu_3\text{-}OH)_2(L_6)_4(NO_3)_2]\cdot MeCN$ (**8**). The analogous complexes **6** and **7** crystallise in the triclinic $P\bar{1}$ space group ($Z = 1$) and each exhibits a butterfly-like $[M_4O_2]$ core whereby the body and wing-tip M(II) (M = Co, Ni) centres are connected by two μ_3-OH^- ions (O1(H1) and s.e.). Inversion centres lie at the midpoint of the Co2···Co2 and Ni2···Ni2 vertices in **6** and **7**, respectively. The Co(II) oxidation states in **6** were confirmed using BVS calculations and charge balancing considerations (Table S3†). In both **6** and **7**, two of the four singly deprotonated L_5^- ligands exhibit $\eta^1{:}\eta^2{:}\eta^1$ μ-bonding modes while the remaining two demonstrate $\eta^1{:}\eta^2$ μ-bridging arrays whereby their methoxy functional groups forge long contacts with nearby Co(II) and Ni(II) centres (Co1···O3 = 2.58 Å and Ni1···O5 = 2.31 Å), respectively. The remaining metal centres are six coordinate distorted octahedral sites (Fig. 6). Terminal water ligands complete the coordination sphere at Co1 at a distance of 2.02 Å (Co1–O6 and s.e.) and Ni1 at a distance of 2.04 Å (Ni1–O6 and s.e.). The protons of these terminal waters also participate in H-bonding with a neighbouring NO_3^- counter anion lying at the periphery of the structures in **6** and **7**. The second nitrate ion in both analogues is situated above the

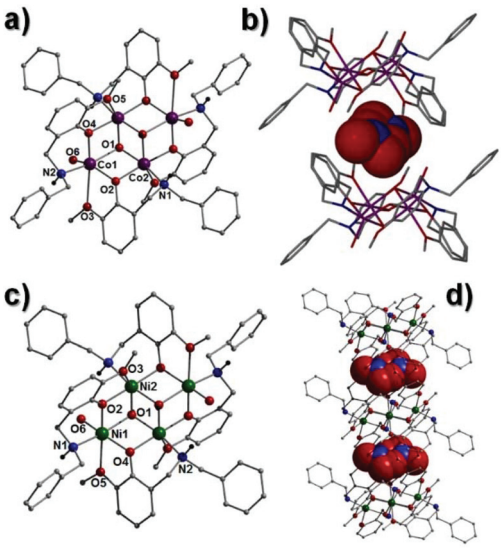

Fig. 6 (Left) Crystal structures of $[(NO_3)\subset Co(II)_4(\mu_3\text{-}OH)_2(L_5)_4(H_2O)_2](NO_3)\cdot H_2O$ (**6**; a) and $[(NO_3)\subset Ni(II)_4(\mu_3\text{-}OH)_2(L_5)_4(H_2O)_2](NO_3)\cdot H_2O$ (**7**; c). (Right) Space-fill representations of the disordered NO_3^- guests within the molecular cavities formed by two $\{Co(II)_4\}$ metallocalix[4]arene units in **6** (b) and three $\{Ni(II)_4\}$ units in **7** (d). Hydrogen atoms and waters of crystallisation have been omitted for clarity in all cases.

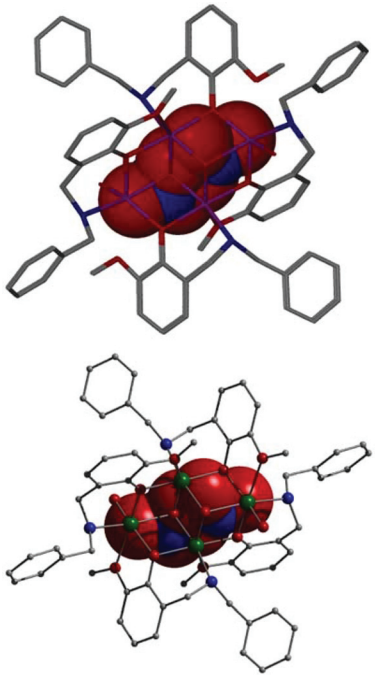

Fig. 7 Crystal structures of **6** and **7** as viewed perpendicular to the $\{Co(II)_4\}$ plane (top) and $\{Ni(II)_4\}$ plane (bottom). Disordered NO_3^- counter anions are represented in space-fill mode. Hydrogen atoms and waters of crystallisation have been omitted for clarity.

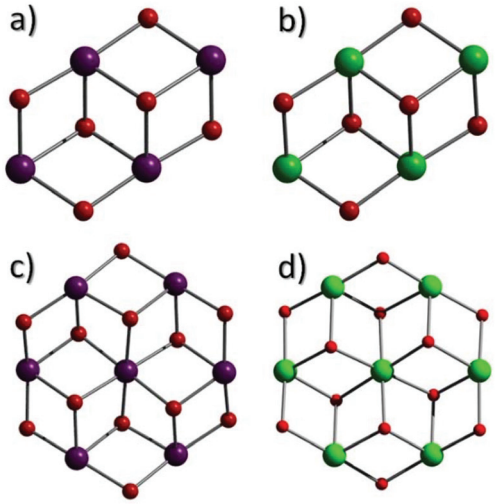

Fig. 8 The "butterfly" inorganic $\{Co(II)_4(\mu_3\text{-}OH)_2\}^{6+}$ and $\{Ni(II)_4(\mu_3\text{-}OH)_2\}^{6+}$ cores in **6** (a), **7** and **8** (b). The heptanuclear $\{Co(III)Co(II)_6(\mu_3\text{-}OH)_6\}^{9+}$ and $\{Ni(II)_6(\mu_3\text{-}OH)_6\}^{8+}$ cores as observed in the original pseudo metallocalix[6]arene complexes $[(NO_3)\subset Co(III)Co(II)_6(\mu_3\text{-}OH)_6(L_2)_6](NO_3)_2$ (**2**, c) and $[Ni(II)_7(\mu_3\text{-}OH)_6(L_1)_6](NO_3)_2$ (**1**, d).[1] Colour code: Co (purple), Ni (green), O (red).

planar $\{M(II)_4\}$ (M = Co, Ni) cores and are disordered over two sites (50 : 50 occupation and related by a centre of inversion; see crystallographic section for details) (Fig. 7).

The topologies in complexes **6** and **7** also share other structural similarities to that of the heptanuclear metallocalix[6]arene $[(NO_3)\subset Co(III)Co(II)_6(\mu_3\text{-}OH)_6(L_2)_6](NO_3)_2$ (**2**). More specifically and as with the L_2^- ligands in **2** (Scheme 1b), the four singly deprotonated L_5^- ligands in **6** and **7** sit alternately above and below their planar $\{M(II)_4(\mu_3\text{-}OH)_2\}^{6+}$ (M = Co, Ni) cores. This gives rise to pseudo metallocalix[4]arene topologies in both analogues, where one of the two previously described NO_3^- counter anions occupies the molecular cavity formed by two superimposed $\{M(II)_4\}$ (M = Co, Ni) units as they stack along the *a* axis of the unit cells in both **6** and **7** (Fig. 6b and d). These nitrate anions (labelled N3 and O7–9 and both cases) are held in position through H-bonding interactions with protons of nearby μ_3-bridging OH^- ions (O1) and ligated waters (O6) at distances of O1(H1)···O9 = 1.83 Å and O6(H6B)···O7 = 1.82 Å in **6** and O1(H1)···O8 = 1.84 Å and O6(H6A)···O7 = 1.85 Å in **7**.

Note that the planar inorganic cores in **6** and **7** may also be described as comprising half of a $\{M(II)_7(\mu_3\text{-}OH)_6\}^{8+}$ (M = Co, Ni) unit as exhibited in **1** (or $\{Co(III)Co(II)_6(\mu_3\text{-}OH)_6\}^{9+}$ in **2**), and highlighted in Fig. 8. Indeed, we can assume from these findings that the employment of ligand L_5H has sterically hindered core growth, leading to the formation of the tetrametallic cores in **6** and **7** as opposed to the larger heptametallic core observed (for instance in **2**) when using the 2-iminophenyl-6-methoxyphenol ligand (L_2H in Scheme 1). This overcrowding and resultant nuclearity change is caused by the introduction of the (distorted) trigonal pyramidal secondary amine group along with the additional aliphatic carbon atom. The result is a much more distorted ligand shape and although a planar $\{M_x(\mu_3\text{-}OH)_y\}$ (M = Co, Ni) core is achieved, its size has been limited accordingly.

The tetranuclear butterfly $\{Ni(II)_4\}$ core in **7** is once again observed upon construction of the complex $[Ni(II)_4(\mu_3\text{-}OH)_2(L_6)_4(NO_3)_2]\cdot MeCN$ (**8**) (Fig. 9). Complex **8** was obtained from the reaction of $Ni(NO_3)_2\cdot 6H_2O$ and L_6H (Br analogue of L_5H) in the presence of a suitable base (NaOH) using either MeOH or MeCN as solvent (see Experimental section for details). Complex **8** crystallises in the triclinic $P\bar{1}$ space group and comprises two half $\{Ni(II)_4\}$ units in the asymmetric unit, each of which exhibit an independent inversion centre located at the midpoint of the Ni2···Ni2 and Ni4···Ni4 vectors, respectively. Furthermore, a single MeCN solvent of crystallisation sits on a general position within the asymmetric unit in **8**. Akin to **6** and **7**, the butterfly cores in **8** are connected by two μ_3-bridging OH^- ions (O5 and s.e.; O105 and s.e.) and a combination of $\eta^1{:}\eta^2{:}\eta^1$ μ- and $\eta^1{:}\eta^2$ μ-bridging L_6^- ligands (Fig. 8 and 9). However, complex **8** does differ from **6** and **7** in that the NO_3^- counter anions do not sit within the molecular cavities in **8**, instead occupying the remaining ligation spots at the distorted octahedral metal centres (Ni1 and Ni3) through chelation. This significant difference gives rise to a different packing topology in **8** (*cf.* **6** and **7**). Here, the individual $\{Ni(II)_4\}$ units are connected to one another through H-bonding interactions between their μ_3-OH^- protons and Br^- groups of neighbouring cages (*e.g.* O105(H105)···Br2 = 2.63 Å and O5(H5)···Br4 = 2.64 Å; Fig. S10†).

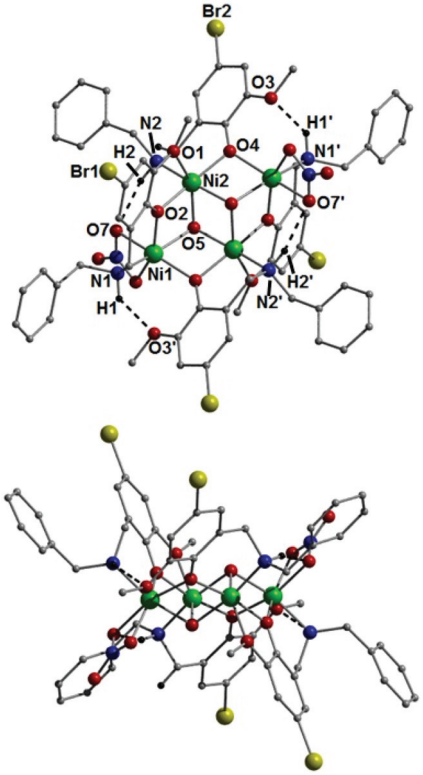

Fig. 9 Crystal structure of one of the two $[Ni(II)_4(\mu_3\text{-}OH)_2(L_6)_4](NO_3)_2$ units observed in the a.s.u. of **8** as viewed perpendicular (top) and parallel (bottom) to the $\{Ni_4\}$ plane. The solvents of crystallisation and the majority of hydrogen atoms have been omitted for clarity. Dashed lines represent intramolecular H-bonds at distances (Å): N1(H1)···O3′ = 2.192 and N2(H2)···O7′ = 2.229.

Intramolecular H-bonds are observed between the tertiary amine protons and chelating NO_3^- counter anions (*i.e.* N2(H2)···O7 = 2.162 Å and N102(H102)···O107 = 2.11 Å) and oxygen atoms belonging to OMe groups on each L_6^- unit (N1(H1)···O3 = 2.14 Å and N101(H101)···O103 = 2.16 Å). Intermolecular interactions also arise between aromatic L_6^- protons (*i.e.* H3 and H127) and chelating NO_3^- anions (*i.e.* O8) at distances of (Å): 2.48 (C3(H3)···O8) and 2.60 (C127(H127)···O8). Weak intermolecular H-bonding also occurs between the protons of aromatic rings (*i.e.* H11) and OMe groups (H16A) of the L_6^- ligands with juxtaposed Br atoms also belonging to nearby ligand units (C16(H16A)···Br1 = 3.03 Å and C11(H11)···Br1 = 2.98 Å). The individual $\{Ni(II)_4\}$ units in **8** pack in a brickwork manner as shown in Fig. S11.†

Magnetic studies

The dc (direct current) molar magnetic susceptibility, χ_M, of polycrystalline samples of **3**, **6** and **8** was measured in an applied magnetic field, B, of 0.1 T, in the T = 2–300 K temperature range. The experimental results are shown in Fig. 10 in the form of the $\chi_M T$ products, where $\chi = M/B$, and M is the magnetisation of the sample.

For **3**, the $\chi_M T$ product of 2.10 cm^3 mol^{-1} K at T = 280 K is close to that expected for two non-interacting Ni(II) ions

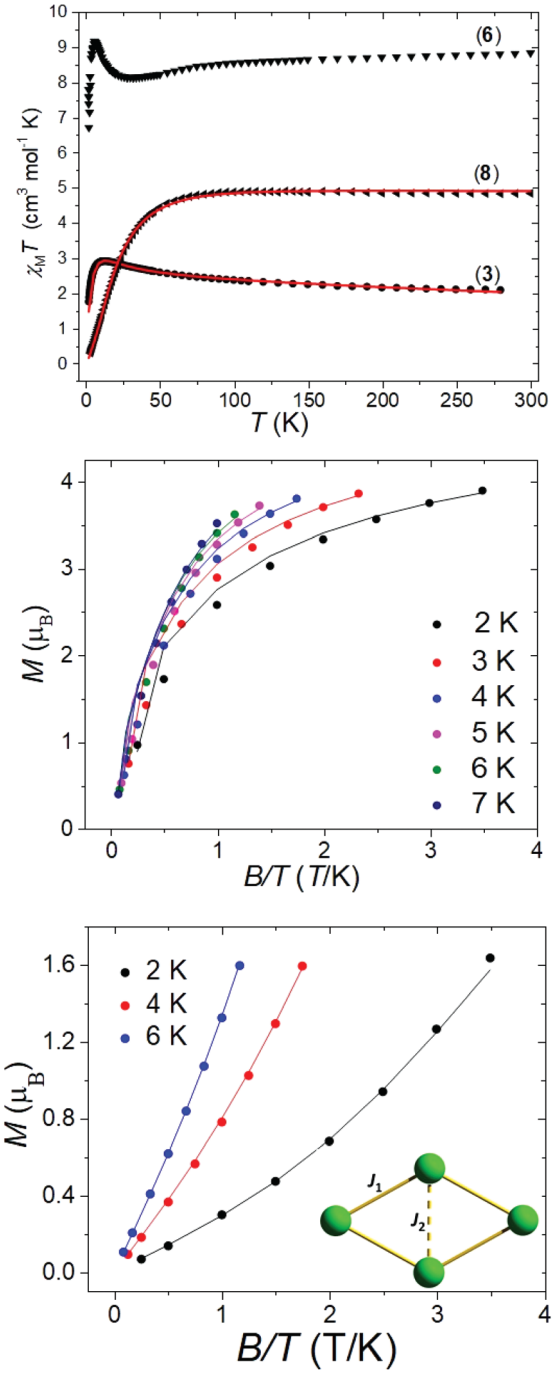

Fig. 10 Top: Plot of $\chi_M T$ *versus* T for complexes **3**, **6** and **8**. Middle: Reduced magnetisation data for complex **3**. Bottom: Reduced magnetisation data for complex **8**. The inset shows the exchange coupling scheme used to fit the data; $\hat{H} = -2J_1(\hat{S}_1\cdot\hat{S}_2 + \hat{S}_2\cdot\hat{S}_3 + \hat{S}_3\cdot\hat{S}_4 + \hat{S}_4\cdot\hat{S}_1) - 2J_2(\hat{S}_2\cdot\hat{S}_4)$. The solid lines represent a simultaneous best-fit of the experimental susceptibility and magnetisation data as described in the main text.

(2.40 cm^3 mol^{-1} K) assuming g_{Ni} = 2.2, where g_{Ni} is the g-factor of Ni(II). Upon cooling, the value of $\chi_M T$ increases reaching a maximum of 2.93 cm^3 mol^{-1} K at 13 K, before decreasing to 1.76 cm^3 mol^{-1} K at 2 K. This increase is indicative of weak

intramolecular ferromagnetic exchange interactions between the phenoxo-bridged Ni(II) ions, with the sharp decrease in the value of $\chi_M T$ at low temperature attributed to antiferromagnetic intermolecular interactions between neighbouring dimers and/or zero-field splitting (zfs) effects. The susceptibility and magnetisation data (Fig. 10, middle) were fitted simultaneously using the program PHI and a spin-Hamiltonian of the form:[24,25]

$$\hat{H} = -2\sum_{i,j>i}^{n} \hat{S}_i J_{ij} \hat{S}_j + \mu_B \sum_{i=1}^{n} \vec{B} g_i \hat{S}_i + \sum_{i=1}^{n} D\left[\hat{S}_{z,i}{}^2 - S_i(S_i+1)/3\right] \quad (1)$$

where $\hat{S}$ is a spin operator, J is the pairwise isotropic magnetic exchange interaction between constitutive N(II) centres, μ_B is the Bohr magneton, $\vec{B}$ the external static magnetic field, g the isotropic g-factor of Ni(II) (fixed to $g = 2.2$; see EPR section below), the indices i and j refer to the two Ni ions ($n = 2$ for **3**), D is the second-order single-ion uniaxial anisotropy parameter of Ni(II) and $\hat{S}_{z,i}{}^2$ is the Cartesian component of spin operator $\hat{S}$ of the i^{th} Ni(II) centre along the z-direction of the local coordinate frame. The best-fit parameters obtained were $2J$ = 7.70 cm^{-1} and D_{Ni} = 7.42 cm^{-1} (Fig. S13† shows the corresponding Zeeman energy diagram). These values are close to that obtained from simulations of the EPR spectra (*vide infra*). The fit of the susceptibility data can be improved marginally through the addition of an intermolecular interaction, zJ' = −0.09 cm^{-1}. Examples of ferromagnetically coupled phenoxo-bridged Ni(II) dimers are rather rare,[26,27] with most being either heteroleptic,[28,29] or homoleptic and possessing Ni–O–Ni bridging angles less than 99°.[30] Note that the asymmetric Ni–O–Ni bridging angles in **3** are of 96.11° and 101.77°.

The susceptibility data for **6** and **8** are also given in Fig. 10. The $\chi_M T$ value of **8** at 300 K is 4.85 $cm^3\ mol^{-1}$ K which is in excellent agreement with the expected high temperature value for four $S = 1$ ions (g_{Ni} = 2.2, $\chi_M T$ = 4.84 $cm^3\ mol^{-1}$ K). Upon cooling, the value of $\chi_M T$ remains essentially constant until approximately 60 K where it begins to decrease rapidly reaching a minimum of 0.150 $cm^3\ mol^{-1}$ K at 2 K. This behaviour is indicative of weak antiferromagnetic exchange between the metal ions, and/or zfs effects. The susceptibility and magnetisation data were fit simultaneously as described above using the exchange coupling scheme depicted in the inset of Fig. 10 (bottom). The best-fit parameters obtained were $2J_1$ = −5.68 cm^{-1}, $2J_2$ = 35.70 cm^{-1} and D_{Ni} = 12.43 cm^{-1} (see Fig. S14† for the corresponding Zeeman energy diagram for **8**).

The coupling constants obtained are in line with those derived for previously published, structurally analogous [Ni(II)$_4$] systems; the dominant structural parameter being the average Ni–O–Ni angles in the butterfly.[30] Ferromagnetic exchange interactions would be expected for Ni–O–Ni angles <99° (Ni2–O–Ni4, ~95°), with antiferromagnetic exchange interactions at Ni–O–Ni angles >99° (Ni1–O–Ni4 and Ni2–O–Ni3, ~99°; Ni1–O–Ni2 and Ni3–O–Ni4, ~98–105°).[31,32] The D_{Ni} value extracted from the fits is in the same range as that found in **3** and that previously reported for Ni(II) ions in a distorted octahedral environment with similar donor atoms (Fig. 9).[33]

For **6** the value of $\chi_M T$ at 300 K is 8.84 $cm^3\ mol^{-1}$ K (Fig. 10), a value close to that expected for four non-interacting Co(II) ions ($S = 3/2$, g_{Co} = 2.2, $\chi_M T$ = 9.07 $cm^3\ mol^{-1}$ K). Upon cooling the value of $\chi_M T$ decreases, reaching a minimum of 8.14 $cm^3\ mol^{-1}$ K at 28 K, before increasing to a maximum value of 9.18 $cm^3\ mol^{-1}$ K at 6 K, and then decreasing to 6.72 $cm^3\ mol^{-1}$ K at 2 K. This behaviour is commonly observed for complexes containing octahedral Co(II) ions: the initial decrease in $\chi_M T$ is due to the orbital contribution of the Co(II) ions, the increase to the maximum at $T = 6$ K due to the presence of some ferromagnetic interactions, with the decrease below this temperature attributed to antiferromagnetic exchange interactions and/or zfs effects.[34–37] Magnetisation data (Fig. S15†) is consistent with the presence of competing F/AF exchange and the presence of significant anisotropy. First order spin orbit coupling effects associated with the octahedral Co(II) ion preclude any simple quantitative analysis of the data. No out-of-phase ac signals were observed for **6**, even in the presence of an applied dc field.

MF/HF EPR spectroscopy

In order to refine the values obtained from the fitting of the magnetic measurements for complex **3**, multi-frequency/high-field EPR was employed on a powdered and pelletised sample. Spectra were recorded at several frequencies ranging from 95 to 662 GHz and in the temperature range 5–25 K (Fig. 11 and Fig. S16 and S17†). For all frequencies, only a few signals were observed whose intensities change with temperature. At 331 and 442 GHz, besides the strong forbidden transition (at ~2.55 and ~3.88 T, respectively), small signals at higher fields (9 to 10 T at 331.2 GHz and 12 to 14 T at 442 GHz) were also recorded. These permitted signals are attributed to the accessing of successive energy levels from the lowest level group (which would belong to the $S = 2$ multiplet in the strong coupling limit) for the y orientation. For the frequency ranges 95–110 GHz and 220–255 GHz, we observe close to zero signals, which are indicative of the existence of gaps in the spin energy diagram, of approximately 3.3 and 7.3 cm^{-1}, respectively. The structure of the spectra does not allow for a simple analysis, as expected from the results of the magnetic measurements, which suggest that $|D_1|$, $|D_2|$ and $|2J|$ are comparable (for comparative purposes see Fig. S18† for simulations using a Giant spin description with a simple $S = 2$ model). Simulations of the spectra were thus performed in the frame of the following Hamiltonian for a coupled Ni(II) dimer:

$$H = \mu_B g B \cdot (\hat{S}_1 + \hat{S}_2) - 2J\hat{S}_1 \cdot \hat{S}_2 + D_1(\hat{S}_{1z}{}^2 - S(S+1)/3) + E_1(\hat{S}_{1x}{}^2 - \hat{S}_{1y}{}^2) + D_2(\hat{S}_{2z}{}^2 - S(S+1)/3) + E_2(\hat{S}_{2x}{}^2 - \hat{S}_{2y}{}^2) \quad (2)$$

where μ_B is the Bohr magneton, g is the single ion g-value, J is the magnetic exchange parameter, S is the spin quantum number, and D and E are the ZFS axial and rhombic parameters, respectively. In order to avoid over parameterization,

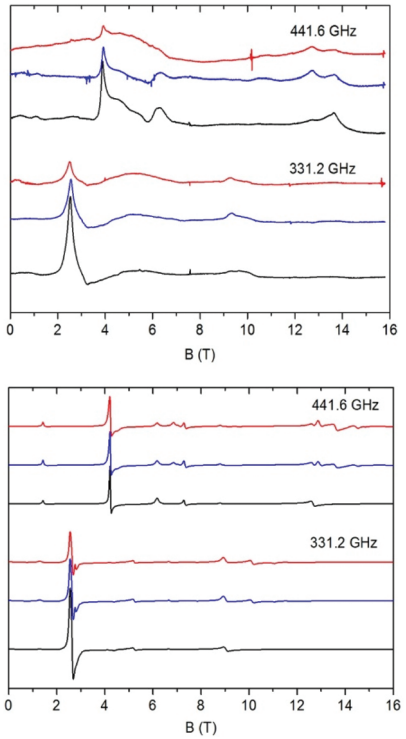

Fig. 11 Experimental (top) and simulated (bottom) MF/HF-EPR spectra obtained on a polycrystalline pelletised sample of $[Ni(II)_2(L_3)_3(H_2O)](NO_3)\cdot 3MeOH\cdot H_2O$ (**3**) at frequencies of 331.2 and 441.6 GHz and temperatures of 25 K (red line), 15 K (blue line) and 5 K (black line).

the description of the system is simplified significantly, due to the reduced number of (independent) transitions detected in the experimental spectra. The assumption of the collinearity of both ZFS tensors is the most drastic. In addition, both g values were taken as identical and the anisotropy of the g factors neglected. These last approximations are expected to affect the calculated spectra much less, due to the masking effect of the ZFS terms over variations of the Zeeman effect. Simulations of the experimental spectra, for which the resonance positions are rather well reproduced (Fig. 11), were obtained for the following set of parameters: $D_1 = 10(1)$ cm^{-1}, $E_1 = 2.5(6)$ cm^{-1}, $D_2 = 9(1)$ cm^{-1}, $E_2 = 2.25(65)$ cm^{-1}, $g_1 = g_2 = g = 2.2(2)$ and $2J = 7.5(1.5)$ cm^{-1}. The D_i (i = 1, 2) and $2J$ values obtained compare well with those obtained from the magnetic studies. The E_i values reported have been chosen, among the possible sets of values, so that they lead to the same E_i/D_i ratio. Indeed, the three or four lowest energy levels of the system behave very similarly to changes on E_i if $E_1 + E_2$ is constant. One may notice a discrepancy in the temperature behaviour of the signals associated to the y orientation at 331 and 442 GHz. This can be corrected through a change on E_i (i = 1, 2) values, at the expense of worsening the simulation of the low field signals (observed at 110 and 220–255 GHz frequencies). Despite our best efforts, it has not been possible to find parameters fully satisfying all the identified signals, most probably as a result of the (over) simplified model used. Finally, the spectra clearly shows that the magnetic anisotropy of **3** is rather rhombic ($E_i/D_i = 0.25$) for both Ni(II) ions.

Conclusions

We have described the synthesis and characterisation of a family ligands including 2-methoxy-6-{[(2-methoxyphenyl) imino]methyl}phenol (L_3H), 2-[(benzylimino)methyl]-6-methoxyphenol (L_4H), 2-[(benzylamino)methyl]-6-methoxyphenol (L_5H) and 2-[(benzylamino)methyl]-4-bromo-6-methoxyphenol (L_6H). Their subsequent complexation with Co(II) and Ni(II) ions gave rise to the dimetallic complex $[Ni(II)_2(L_3)_3(H_2O)](NO_3)\cdot 2H_2O\cdot 3MeOH$ (**3**); the monometallic $[Ni(II)(L_4)_2]$ (**4**) and $[Co(III)(L_4)_3]\cdot H_2O\cdot MeOH$ (**5a**) species along with the tetranuclear siblings $[(NO_3)\subset Co(II)_4(\mu_3\text{-}OH)_2(L_5)_4(H_2O)_2](NO_3)\cdot H_2O$ (**6**), $[(NO_3)\subset Ni(II)_4(\mu_3\text{-}OH)_2(L_5)_4](NO_3)\cdot H_2O$ (**7**) and $[Ni(II)_4(\mu_3\text{-}OH)_2(L_6)_4(NO_3)_2]\cdot MeCN$ (**8**). Complexes **3–8** represent the first examples of transition metal coordination of ligands $L_{3-6}H$. The inorganic planar cores in **6–8** $(\{M(II)_4(\mu_3\text{-}OH)_2\}^{6+}$ (M = Co and Ni)) may be viewed as fragments of the $\{M(II)_7(\mu_3\text{-}OH)_6\}^{8+}$ (M = Co, Ni) and $\{Co(III)Co(II)_6(\mu_3\text{-}OH)_6\}^{9+}$ cores observed within our previously reported pseudo metallocalix[6]arenes,[1] which were constructed using similar Schiff base ligands (L_1H and L_2H in Scheme 1). Indeed, we have demonstrated here that the combination of $M(II)(NO_3)_2\cdot 6H_2O$ (M = Co(II) and Ni(II)) and NaOH promotes double hydroxide layer brucite-like sheet formation whose growth/size is limited by the "cookie cutter" Schiff base ligands employed in this work. Moreover, we have highlighted that careful ligand selection can be used to introduce more synthetic control in the production of planar μ_3-OH bridged Ni(II) and Co(II) polymetallic cages.

SQUID measurements on $[Ni(II)_2(L_3)_3(H_2O)](NO_3)\cdot 3MeOH\cdot H_2O$ (**3**) reveal weak ferromagnetic exchange interactions between the two Ni(II) ions; a simultaneous fit of the susceptibility and magnetisation data affording $2J = 7.70$ cm^{-1} and $D_{Ni} = 7.42$ cm^{-1}, in agreement with simulations of the EPR data. Complex **3** is therefore a rather rare example of a ferromagnetically coupled diphenoxo-bridged $[Ni(II)_2]$ complex, especially given the unusual Ni–O–Ni bridging angles. Even if it has not been possible to obtain a fully reliable set of parameters from the MF/HF EPR spectra of (**3**), the analysis of the spectra does confirm the ferromagnetic character of the coupling. Indeed, the forbidden transition evolves with a g_{eff} value close to 8 and more generally the spectra exhibit similarities with the $S = 2$ spectra obtained for the strong coupling limit of the single ion parameters. This is because the signals observed come from the lowest energy levels, corresponding to the $S = 2$ levels in the strong coupling limit. However, changing the J value modifies the resonance positions.

The best fit of the susceptibility and magnetisation data of $[Ni(II)_4(\mu_3\text{-}OH)_2(L_6)_4(NO_3)_2]\cdot MeCN$ (**8**), assuming a butterfly-like structure incorporating two different exchange interactions (wing–body and body–body) provided $2J_1 = -5.68$ cm^{-1}, $2J_2 = 35.70$ cm^{-1} and $D_{Ni} = 12.43$ cm^{-1}, values entirely consistent

with previously published data on complexes with a similar diamond-like arrangement of the metal ions. The tetrameric $[(NO_3)\subset Co(II)_4(\mu_3\text{-}OH)_2(L_5)_4(H_2O)_2](NO_3)\cdot H_2O$ (**6**) cluster demonstrates competing anti- and ferromagnetic exchange along with significant anisoptropy.

Experimental

Infra-red spectra for complexes **6–8** were recorded on a PerkinElmer FT-IR Spectrum 100 spectrometer, while spectra for **3–5** were obtained from a newly acquired Bruker Alpha FT-IR Platinum ATR spectrometer (School of Natural Sciences, Bangor University). Elemental analysis was carried out at OEA Laboratories Ltd (Kelly Bray, Cornwall, UK). MALDI TOF-MS measurements on complexes **6** and **8** were carried out at the EPSRC UK National Mass Spectrometry Facility at Swansea University. Powder XRD was carried out using a PANalytical Philips ẊPert 3040/60 diffractometer at 45 kV and 35 mA between 5 and 60° 2θ using Ni-Filtered Cu–$K_{\alpha1}$ radiation (λ = 1.5405 Å) at the School of Natural Sciences, Bangor University.

Variable-temperature, solid-state direct current (dc) and alternating current (ac) magnetic susceptibility data down to 2 K were collected on a Quantum Design MPMS-XL SQUID magnetometer and a Quantum Design PPMS magnetometer fitted with an ac measurement system, respectively. Diamagnetic corrections were applied to the observed paramagnetic susceptibilities using Pascal's constants. All measured complexes were set in eicosane to avoid torqueing of the crystallites. All magnetic samples were collected as single-crystalline products and analysed using microanalysis and IR measurements prior to their magnetic assessment. Phase purity between cross-batches were validated using unit cell checks and IR measurements.

MF/HF-EPR measurements were performed on a multi-frequency spectrometer operating in a double-pass configuration. A 110 GHz frequency source (Virginia Diodes Inc.) alone or with multipliers up to the 6th harmonic), as well as 95 GHz and 115 GHz Gunn oscillators (Radiometer Physics GmbH) together with a quadrupler or a quintupler were used. The measurements were done on powdered samples pressed into pellets in order to limit torqueing effects. Calculated spectra were obtained with the SIM program from H. Weihe (Univ. of Copenhagen).

Crystallography

All complexes were collected on an Rigaku AFC12 goniometer equipped with an enhanced sensitivity (HG) Saturn724+ detector mounted at the window of an FR-E+ Super Bright molybdenum rotating anode generator with HF Varimax optics (100 m focus) (CCDC numbers: 1874840–1874846†). The cell determination and data collection of all complexes were carried out using the CrystalClear-SM Expert package (Rigaku, 2012). Each data reduction, cell refinement and absorption correction were carried out using CrysAlisPro software (Rigaku OD, 2015),[38] while all structures were initially solved and refined using SHELXT and SHELXL-2014[39] within OLEX-2.[40] All structures were refined and completed in-house by full matrix least squares using SHELXL-14[39] and refined with OSCAIL packages.[41]

Collection and refinement details

Due to modelling difficulties, the residual electron densities representing solvent entities within the solvent accessible voids (total volume = 971 Å^3) in **3** were removed from the structure using the SQUEEZE program.[42] The NO_3^- counter anion required the DFIX, DANG and FLAT restraints and remained isotropic. All protons in **3** were assigned to calculated positions. All non hydrogen atoms were modelled as anisotropic in **4**, while all hydrogen atoms were assigned to calculated positions. The SQUEEZE program was also employed in the treatment of **5a**, giving a total void volume of 551 Å^3 and resulting in the removal of 55 electrons from the structure. This electron density has been assigned as representing 1 × MeOH and 1 × H_2O solvent molecule per [Co_1] molecule (Z = 2).

The μ_3-bridging $^-$OMe ions in **5b** were best modelled as sharing 50 : 50 occupancy with bridging $^-$OH moieties. At two of these positions, half occupancy waters of crystallisation (labelled O50 and s.e.) lie above these bridging $^-$OMe/$^-$OH ions and are presumed to partake in H-bonding with the $^-$OH moieties at distances of 2.84 Å (O18···O50). DFIX restraints were employed on the O–CH_3 distances of all bridging –OMe functional groups in **5b**. All non-hydrogen atoms in **5b** apart from the bridging $^-$OMe carbons (labelled C46–C48 and C94–96) were refined anisotropically and all protons were assigned to calculated positions. Due to modelling difficulties the residual electron densities representing NO_3^- counter anions and solvent entities within the solvent accessible voids (total volume ~1911 Å^3; ~77 electrons per cage) in **5b** were modelled using the SQUEEZE program to give the final formula $[Co(II)_7(OMe)_6(L_4)_6](NO_3)_2\cdot 0.5H_2O\cdot 4MeOH$.[42]

All non-hydrogen atoms in complexes **6** and **7** were modelled as anisotropic. Both the NO_3^- counter anions in **6** were restrained using the DFIX command. The $^-$OH proton (H1) and the terminal water protons (H6A and H6B) in **6** were assigned to calculated positions, while the corresponding water protons in **7** (H6A and H6B) were located in the difference map. All other protons were assigned to calculated positions. In complexes **6** and **7**, both nitrates were found to be disordered over two sites (one of which lies at a special position while the other shares space with a water of crystallisation (labelled O7A in **6** and O13 in **7**). Both were modelled at half occupancy. The selected single crystal in **8** contains light green hexagonal plates. Most crystals within the sample looked twinned and gave multicomponent diffraction patterns. A small clean fragment was selected for collection. Large residual electron density peaks observed were attributed to small twin domains within the crystal, which contributed to the observed diffraction pattern.

Preparation of complexes

All reactions were performed under aerobic conditions and all reagents and solvents were used as purchased. *Caution*:

Although no problems were encountered in this work, care should be taken when manipulating the potentially explosive nitrate salts.

Synthetic procedures

Synthesis of $[Ni(II)_2(L_3)_3(H_2O)](NO_3)\cdot 2H_2O\cdot 3MeOH$ (3). $Ni(NO_3)_2\cdot 6H_2O$ (0.25 g, 0.85 mmol), L_3H (0.22 g, 0.85 mmol) and NaOH (0.034 g, 0.85 mmol) were dissolved in methanol (30 cm^3) and stirred for 4 hours. The resultant lime green solution was filtered and X-ray quality crystals of **3** were obtained upon slow evaporation in 30% yield after 3 weeks. Elemental analysis (%) calculated (found) for **3** ($C_{48}H_{58}N_4O_{17}Ni_2$): C 53.36 (53.40), H 5.41 (4.81), N 5.19 (5.37). FT-IR (cm^{-1}): 3368 (vb), 3056 (w), 2942 (w), 2834 (w), 1611 (s), 1588 (s), 1541 (m), 1493 (s), 1467 (s), 1441 (s), 1384 (s), 1336 (s), 1297 (s), 1228 (s), 1192 (s), 1173 (s), 1118 (m), 1078 (m), 1046 (m), 1011 (m), 974 (m), 870 (w), 850 (w), 828 (w), 785 (m), 742 (s), 638 (m), 587 (m), 527 (m), 474 (w), 440 (w), 425 (w).

Synthesis of $[Ni(II)(L_4)_2]$ (4). $Ni(NO_3)_2\cdot 6H_2O$ (0.25 g, 0.85 mmol), L_4H (0.20 g, 0.85 mmol) and NaOH (0.034 g, 0.85 mmol) were dissolved in methanol (30 cm^3) and stirred for 4 hours. The resultant lime green solution was filtered and X-ray quality crystals of **4** were obtained upon slow evaporation in 25% yield after 2 weeks. Elemental analysis (%) calculated (found) for **4** ($C_{30}H_{28}N_2O_4Ni_1$): C 66.82 (66.56), H 5.23 (4.98), N 5.20 (5.12). FT-IR (cm^{-1}): 3464 (b), 3055 (w), 3020 (w), 2928 (w), 2903 (w), 2852 (w), 2828 (w), 1836 (w), 1615 (s), 1551 (m), 1495 (m), 1471 (s), 1452 (s), 1434 (s), 1399 (m), 1332(m), 1319 (m), 1241 (s), 1164 (m), 1115 (w), 1094 (w), 1056 (m), 1031 (m), 984 (w), 957 (m), 914 (w), 874 (m), 858 (w), 791 (w), 762 (m), 737 (s), 699 (s), 656 (m), 602 (w), 524 (w), 490 (m), 447 (m), 417 (m).

Synthesis of $[Co(III)(L_4)_3]\cdot H_2O\cdot MeOH$ (5a) and $[Co(II)_7(OMe)_6(L_4)_6](NO_3)_2\cdot 0.5H_2O\cdot 4MeOH$ (5b) co-crystals. $Co(NO_3)_2\cdot 6H_2O$ (0.25 g, 0.85 mmol), L_4H (0.20 g, 0.85 mmol) and NaOH (0.034 g, 0.85 mmol) were dissolved in methanol (30 cm^3) and stirred for 4 hours. The resultant purple solution was filtered and X-ray quality crystals of **5a** (purple) and **5b** (red) were obtained upon slow evaporation of the mother liquor after 3 weeks.

Sole synthesis of $[Co(III)(L_4)_3]\cdot H_2O\cdot MeOH$ (5a). $Co(NO_3)_2\cdot 6H_2O$ (0.25 g, 0.86 mmol) was dissolved in methanol (30 cm^3) along with one equivalent of hydrogen peroxide (1 cm^3, 0.86 mmol). The resultant purple solution was then introduced to L_4H (0.20 g, 0.85 mmol) and NaOH (0.034 g, 0.85 mmol). X-ray quality crystal of **5a** were obtained upon slow evaporation in 25% yield after 2 weeks. Elemental analysis (%) calculated (found) for **5a**$\cdot H_2O$ ($C_{46}H_{48}N_3O_8Co_1$): C 65.17 (65.15), H 5.94 (5.58), N 4.96 (5.00). FT-IR (cm^{-1}): 3650 (w), 3503 (w), 3325 (w), 2986 (m), 2910 (m), 2821 (w), 2361 (w), 2344 (w), 2028 (w), 1869 (w), 1845 (w), 1802 (w), 1624 (s), 1609 (s), 1595 (s), 1559 (m), 1544 (m), 1508 (s), 1492 (s), 1470 (s), 1437 (m), 1412 (m), 1394 (m), 1342 (s), 1316 (s), 1242 (s), 1221 (s), 1193 (m), 1167 (m), 1109 (m), 1075 (m), 1049 (m), 1035 (m), 1026 (m), 966 (m), 953 (m), 904 (m), 858 (m), 767 (s), 756 (m), 730 (m), 694(m), 638 (m), 624 (m), 600 (m), 575 (m), 541 (m), 497 (w), 483 (w), 450 (w), 434 (w), 424 (w).

Synthesis of $[(NO_3)\subset Co(II)_4(\mu_3\text{-}OH)_2(L_5)_4(H_2O)_2](NO_3)\cdot H_2O$ (6). $Co(NO_3)_2\cdot 6H_2O$ (0.25 g, 0.86 mmol), L_5H (0.21 g, 0.86 mmol) and NaOH (0.034 g, 0.86 mmol) were dissolved in MeCN and the solution stirred at room temperature for 4 hours. X-ray quality crystals of **6** were obtained in 20% yield upon filtration and subsequent slow evaporation of the mother liquor. Elemental analysis (%) calculated (found) for **6**$\cdot 2H_2O$ ($C_{60}H_{76}N_6O_{21}Co_4$): C 49.60 (48.95), H 5.27 (4.97), N 5.78 (6.28). FT-IR (cm^{-1}): 3577 (m), 3502 (m), 3274 (m), 3208 (vb), 3022 (m), 2926 (m), 2855 (m), 1639 (w), 1602 (m), 1579 (m), 1481 (s), 1389 (s), 1359 (s), 1330 (s), 1296 (m), 1255 (m), 1234 (m), 1207 (m), 1087 (m), 1066 (m), 1040 (m), 1028 (m), 1003 (m), 922 (s), 854 (s), 740 (s), 699 (s), 633 (m), 610 (m), 560 (w), 515 (w), 458 (w), 432 (w). MALDI-TOF MS (in DBTC-MeCN matrix) (%, *m*/*z*): 301 (5, $[Co(II)(L_4)]^+$), 364 (81, $[\{[Co(II)(L_4)](NO_3) + H^+\}]$, 637 (12, $[Co(II)_4(\mu_3\text{-}OH)_2(L_4)_4(H_2O)_2]^{2+}$), 664 (100, $[Co(II)_4(\mu_3\text{-}OH)_2(L_4)_4(H_2O)_5]^{2+}$), 755 (42, $[Co(II)_4(\mu_3\text{-}OH)_2(L_5)_4(H_2O)_6(MeCN)_4]^{2+}$), 966 (22, $\{[Co(II)_4(\mu_3\text{-}OH)_4(L_5{}^*)_4(H_2O)_2] + H^+\}$), 1027 (6, $\{[Co(II)_4(\mu_3\text{-}OH)_2(L_5{}^*)_4(H_2O)_2](NO_3)\}^+$), 1055 (25, $\{[Co(II)_4(\mu_3\text{-}OH)_2(L_5{}^*)_4](NO_3)_2 + H^+\}$). *Note*: $L_5{}^* = L_5{}^-\text{-}C_6H_5$ (loss of pendant Ph group).

Synthesis of $[(NO_3)\subset Ni(II)_4(\mu_3\text{-}OH)_2(L_5)_4(H_2O)_2](NO_3)\cdot H_2O$ (7). $Ni(NO_3)_2\cdot 6H_2O$ (0.25 g, 0.86 mmol), L_5H (0.21 g, 0.86 mmol) and NaOH (0.034 g, 0.86 mmol) were dissolved in MeCN and the solution stirred at room temperature for 4 hours. X-ray quality crystals of **7** were obtained in 12% yield upon filtration and subsequent slow evaporation of the mother liquor after 2 weeks. Elemental analysis (%) calculated (found) for **7**$\cdot H_2O$ ($C_{60}H_{74}N_6O_{20}Ni_4$): C 50.25 (50.65), H 5.20 (5.15), N 5.86 (6.19). FT-IR (cm^{-1}): 3576 (w), 3537 (w), 3478 (w), 3268 (w), 3187 (w/vb), 3019 (w), 2841 (w), 1599 (w), 1577 (w), 1478 (s), 1442 (m), 1384 (m), 1360 (m), 1322 (m), 1298 (s), 1256 (m), 1229 (s), 1210 (m), 1168 (w), 1112 (w), 1085 (m), 1072 (w), 1042 (w), 1024 (w), 1001 (m), 921 (w), 880 (m), 851 (w), 817 (w), 778 (w), 768 (w), 739 (s), 697 (s), 643 (w), 633 (w), 614 (m), 555 (w), 540 (w), 519 (w), 493 (w), 460 (w), 433 (w), 416 (w).

Synthesis of $[Ni(II)_4(\mu_3\text{-}OH)_2(L_6)_4(NO_3)_2]\cdot MeCN$ (8). *Method A*: $Ni(NO_3)_2\cdot 6H_2O$ (0.25 g, 0.86 mmol), L_6H (0.28 g, 0.86 mmol) and NaOH (0.0344 g, 0.86 mmol) were dissolved in MeCN and the solution stirred at room temperature for 4 hours. X-ray quality crystals of **8** were obtained in 15% yield upon filtration and subsequent slow evaporation of the mother liquor after 3 weeks. *Method B*: $Ni(NO_3)_2\cdot 6H_2O$ (0.25 g, 0.86 mmol), L_6H (0.28 g, 0.86 mmol) and NaOH (0.0344 g, 0.86 mmol) were dissolved in MeOH and the solution stirred at room temperature for 4 hours. The precipitous solution was then evaporated to dryness and redissolved in MeCN. X-ray quality crystals of **8** were obtained in 18% yield upon filtration and subsequent slow evaporation of the mother liquor. Elemental analysis (%) calculated (found) for **8** ($C_{60}H_{62}N_6O_{16}Br_4Ni_4$): C 42.96 (43.06), H 3.73 (3.76), N 5.01 (4.95). FT-IR (cm^{-1}): 3616 (s), 3268 (s), 3085 (w), 3062 (w), 3028 (w), 3004 (w), 2959 (w), 2937 (w), 2861 (w), 1567 (m), 1484 (s), 1442 (sh), 1358 (m), 1331 (m), 1300 (m), 1247 (m), 1233 (s), 1207 (m), 1095 (m), 1052 (m), 1035 (m), 1019 (m), 1009 (m), 929 (m), 883 (m), 864 (m), 809 (w), 779 (s), 746 (s), 700 (s), 659 (w), 620 (m), 570 (w), 553 (w), 504 (w), 479 (w), 422 (w). MALDI-TOF MS

(in DBTC-MeCN matrix) (%, *m*/*z*): 795 (100, $[Ni(II)_4(\mu_3\text{-}OH)_2(L_6)_4(H_2O)_2]^{2+}$), 820 (12, $[Ni(II)_4(\mu_3\text{-}OH)_2(L_6)_4(MeCN)_2]^{2+}$), 1632 (30, $\{[Ni(II)_4(\mu_3\text{-}OH)_2(L_6)_4(H_2O)] + (NO_3)\}^{+}$).

Conflicts of interest

There are no conflicts to declare.

Acknowledgements

LFJ would like to thank the School of Natural Sciences at Bangor University for their support (MSP, JD and JH). We would like to thank the EPSRC UK National Crystallographic Service (University of Southampton) and EPSRC UK National Mass Spectrometry Facility at Swansea University for their data collection. EKB thanks the EPSRC for funding.

Notes and references

1 (*a*) S. T. Meally, G. Karotsis, E. K. Brechin, G. S. Papaefstathiou, P. W. Dunne, P. McArdle and L. F. Jones, *CrystEngComm*, 2010, **12**, 59; (*b*) S. T. Meally, C. McDonald, G. Karotsis, G. S. Papaefstathiou, E. K. Brechin, P. W. Dunne, P. McArdle, N. P. Power and L. F. Jones, *Dalton Trans.*, 2010, **39**, 4809; (*c*) S. T. Meally, C. McDonald, P. Kealy, S. M. Taylor, E. K. Brechin and L. F. Jones, *Dalton Trans.*, 2012, **41**(18), 5610.

2 (*a*) M. Coletta, R. McLellan, P. Murphy, B. T. Leube, S. Sanz, R. Clowes, K. J. Gagnon, S. J. Teat, A. I. Cooper, M. J. Paterson, E. K. Brechin and S. J. Dalgarno, *Chem. – Eur. J.*, 2016, **22**, 8791–8795; (*b*) T. C. Stamatatos, R. Adam, C. P. Raptopoulou, V. Psycharis, R. Ballesteros, B. Aberca, S. P. Perlepes and A. K. Boudalis, *Inorg. Chem. Commun.*, 2012, **15**, 73–77; (*c*) S. M. Taylor, G. Karotsis, R. D. McIntosh, S. Kennedy, S. J. Teat, C. M. Beavers, W. Wernsdorfer, S. Piligkos, S. J. Dalgarno and E. K. Brechin, *Chem. – Eur. J.*, 2011, **17**, 7521–7530; (*d*) Y. Sunatsuki, H. Shimada, T. Matsuo, M. Nakamura, F. Kai, N. Marsumoto and N. Re, *Inorg. Chem.*, 1998, **37**, 5566–5574.

3 (*a*) A.-A. H. Abu-Nawwas, C. A. Muryn and M. A. Malik, *Inorg. Chem. Commun.*, 2009, **12**, 125–127; (*b*) I.-P. Lorenz, W. Pohl and H. Nöth, *Angew. Chem., Int. Ed. Engl.*, 1997, **36**, 54–56; (*c*) K.-H. Lii and Y.-F. Huang, *Chem. Commun.*, 1997, 839–840.

4 (*a*) N. E. Borisova, Y. A. Ustnyuk, M. D. Reshetova, G. G. Alexsandrov and I. L. Eremenko, *Mendeleev Commun.*, 2003, **13**(5), 202–204; (*b*) G. Aromi, A. S. Batsanov, P. Christian, M. Helliwell, A. Parkin, S. Parsons, A. A. Smith, G. A. Timco and R. E. P. Winpenny, *Chem. – Eur. J.*, 2003, **9**, 5142–5161; (*c*) P. King, R. Clérac, W. Wernsdorfer, C. E. Anson and A. K. Powell, *Dalton Trans.*, 2004, 2670–2676; (*d*) Z. A. Siddiqi, A. Siddique, M. Shahid, M. Khalid, P. K. Sharma, Anjuli, M. Ahmad, S. Kumar, Y. Lan and A. K. Powell, *Dalton Trans.*, 2013, **42**, 9513–9522; (*e*) S. R. Hosseinian, V. Tangoulis, M. Menelaou, C. P. Raptopoulou, V. Psycharis and C. Dendrinou-Samara, *Dalton Trans.*, 2013, **42**, 5355–5366; (*f*) N. E. Borisova, Y. A. Ustnyuk, M. D. Reshetova, G. G. Alexsandrov and I. L. Eremenko, *Mendeleev Commun.*, 2003, **13**(5), 202–204; (*g*) Y.-W. Li, L.-Y. Guo, L. Feng, Z. Jagličič, S.-Y. Zeng and D. Sun, *CrystEngComm*, 2017, **19**, 5897–5906.

5 (*a*) B.-C. Tsai, Y.-H. Liu, S.-M. Peng and S.-T. Liu, *Eur. J. Inorg. Chem.*, 2016, 2783–2790; (*b*) G. Chaboussant, R. Basler, H.-U. Güdel, S. Oschenbein, A. Parkin, S. Parsons, G. Rajaraman, A. Sieber, A. A. Smith, G. A. Timco and R. E. Winpenny, *Dalton Trans.*, 2004, 2758–2766.

6 (*a*) K. F. Konidaris, V. Bekiari, E. Katsoulakou, C. P. Raptapoulou, V. Psycharis, E. Manessi-Zoupa, G. E. Kostakis and S. P. Perlepes, *Dalton Trans.*, 2012, **41**, 3797–3806; (*b*) J. Martinez, I. Aiello, A. Bellusci, A. Crispini and M. Ghedini, *Inorg. Chim. Acta*, 2008, **361**, 2677–2682; (*c*) M. Alexiou, E. Katsoulakou, C. Dendrinou-Samara, E. Manessi-Zoupa, S. P. Perlepes and D. P. Kessissoglou, *Eur. J. Inorg. Chem.*, 2005, 1964–1978; (*d*) J. Hermann and A. Erxleben, *Inorg. Chim. Acta*, 2000, **304**, 125–129; (*e*) A. J. Stemmler, J. F. Kampf and V. L. Pecoraro, *Inorg. Chem.*, 1995, **34**, 2271–2272.

7 P. S. Perlepe, L. Cunha-Silva, V. Bekiari, K. J. Gagnon, S. K. J. Teat, A. Escuer and T. C. Stamatatos, *Dalton Trans.*, 2016, **45**, 10256–10270.

8 M. Mikuriya, K. Tanaka, N. Inoue, D. Yoshioka and J.-W. Lim, *Chem. Lett.*, 2003, **32**, 126–127.

9 (*a*) N. C. Harden, M. A. Bolcar, W. Wernsdorfer, K. A. Abboud, W. E. Streib and G. Christou, *Inorg. Chem.*, 2003, **42**, 7067; (*b*) M. A. Bolcar, S. M. J. Aubin, K. Folting, D. N. Hendrickson and G. Christou, *Chem. Commun.*, 1997, 1485.

10 M. Menelaou, E. Vournari, V. Psycharis, C. P. Raptopoulou, A. Terzis, V. Tangoulis, Y. Sanakis, C. Mateescu and A. Salifoglou, *Inorg. Chem.*, 2013, **52**, 13849–13860.

11 (*a*) E.-C. Yang, Z.-Y. Liu, L. Zhang, N. Yang and X.-J. Zhao, *Dalton Trans.*, 2016, **45**, 8134; (*b*) D.-M. Chen, X.-Z. Ma, X.-J. Zhang, N. Xu and P. Cheng, *Inorg. Chem.*, 2015, **54**, 2976–2982.

12 (*a*) W. L. Leong and J. J. Vittal, *New J. Chem.*, 2010, **34**, 2145–2152; (*b*) K. Mitsumoto, M. Nihei, T. Shiga and H. Oshio, *Chem. Lett.*, 2008, **37**, 966–967.

13 S.-H. Zhang and C. Feng, *J. Mol. Struct.*, 2010, **977**, 62–66.

14 M. Manoli, A. Collins, S. Parsons, A. Candini, M. Evengelisti and E. K. Brechin, *J. Am. Chem. Soc.*, 2008, **130**, 11129–11139.

15 T. D. Keene, M. E. Light, M. B. Hursthouse and D. J. Price, *Dalton Trans.*, 2011, **40**, 2983.

16 (*a*) J. C. Goodwin, R. Sessoli, D. Gatteschi, A. L. Barra, W. Wernsdorfer, A. K. Powell and S. L. Heath, *Dalton Trans.*, 2000, 1835–1840; (*b*) S. L. Heath and A. K. Powell, *Angew. Chem., Int. Ed. Engl.*, 1992, **31**, 191–193.

17 A. V. Pestov, P. A. Slepukhin and Y. G. Yatluk, *Russ. J. Coord. Chem.*, 2011, **37**(8), 619–624.
18 Y.-K. Deng, H.-F. Su, J.-H. Xu, W.-G. Wang, M. Kurmoo, S.-C. Lin, Y.-Z. Tan, J. Jia, D. Sun and L.-S. Zheng, *J. Am. Chem. Soc.*, 2016, **138**, 1328–1334.
19 For the structure of α-$Co(OH)_2$ see: M. Rajamathi, P. Vishnu Kamath and R. Seshadri, *Mater. Res. Bull.*, 2000, **35**, 271–278. For the structure of β-$Co(OH)_2$ see: Ch. Mockenhaupt, Th. Zeiske and H. D. Lutz, *J. Mol. Struct.*, 1998, **443**, 191–196; Z. Liu, R. Ma, M. Osada, K. Takada and T. Sasaki, *J. Am. Chem. Soc.*, 2005, **127**, 13869.
20 D. S. Hall, D. J. Lockwood, C. Bock and B. R. MacDougall, *Proc. R. Soc. A*, 2014, **471**, 20140792.
21 (*a*) M. W. Kanan and D. G. Nocera, *Science*, 2008, **321**, 1072; (*b*) M. W. Kanan, Y. Surendranath and D. G. Nocera, *Chem. Soc. Rev.*, 2009, **38**, 109–114; (*c*) Y. Surendranath, D. A. Lutterman, Y. Li and D. G. Nocera, *J. Am. Chem. Soc.*, 2012, **134**, 6326–6336; (*d*) C. L. Farrow, D. K. Bediako, Y. Surendranath, D. G. Nocera and S. J. L. Billinge, *J. Am. Chem. Soc.*, 2013, 6403–6406; (*e*) M. W. Kanan, J. Yano, Y. Surendranath, M. Dincã, V. K. Yachandra and D. G. Nocera, *J. Am. Chem. Soc.*, 2010, **132**, 13692–13701.
22 (*a*) D. K. Bediako, Y. Surendranath and D. G. Nocera, *J. Am. Chem. Soc.*, 2013, **135**, 3362–3674; (*b*) D. K. Bediako, B. Lasalle-Kaiser, Y. Surendranath, J. Yano, V. K. Yachandra and D. G. Nocera, *J. Am. Chem. Soc.*, 2012, **134**, 6801.
23 A. M. Ullman and D. G. Nocera, *J. Am. Chem. Soc.*, 2013, **135**, 15053.
24 N. F. Chilton, R. P. Anderson, L. D. Turner, A. Soncini and K. S. Murray, *J. Comput. Chem.*, 2013, **34**, 1164–1175.
25 O. Khan, *Molecular Magnetism*, VCH, New York, 1993.
26 R. J. Butcher, C. J. O'Connor and E. Sinn, *Inorg. Chem.*, 1981, **20**, 3486–3493.
27 E. Loukopoulos, B. Berkoff, K. Griffiths, V. Keeble, V. N. Dokorou, A. C. Tsipis, A. Escuer and G. E. Kostakis, *CrystEngComm*, 2015, **17**, 6753–6764.
28 S. Banerjee, M. G. B. Drew, C.-Z. Lu, J. Tercero, C. Diaz and A. Ghosh, *Eur. J. Inorg. Chem.*, 2005, **2005**, 2376–2383.
29 L. Rodríguez, E. Labisbal, A. Sousa-Pedrares, J. A. García-Vázquez, J. Romero, M. L. Durán, J. A. Real and A. Sousa, *Inorg. Chem.*, 2006, **45**, 7903–7914.
30 P. S. Perlepe, A. A. Athanasopoulou, K. I. Alexopoulou, C. P. Raptopoulou, V. Psycharis, A. Escuer, S. P. Perlepes and T. C. Stamatatos, *Dalton Trans.*, 2014, **43**, 16605–16609.
31 A. Das, F. J. Klinke, S. Demeshko, S. Meyer, S. Dechert and F. Meyer, *Inorg. Chem.*, 2012, **51**, 8141–8149.
32 M. A. Halcrow, J.-S. Sun, J. C. Huffman and G. Christou, *Inorg. Chem.*, 1995, **34**, 4167–4177.
33 R. Boča, *Coord. Chem. Rev.*, 2004, **248**, 757–815.
34 R.-X. Yao, X.-H. Qiao, X. Cui, X.-X. Jia and X.-M. Zhang, *Inorg. Chem. Front.*, 2016, **3**, 78–85.
35 X. M. Zhang, J. Q. Li, S. J. Liu, M. B. Luo, W. Y. Xu and F. Luo, *CrystEngComm*, 2014, **16**, 2570–2573.
36 H.-H. Chen, J. Yang, Y.-Y. Liu and J.-F. Ma, *CrystEngComm*, 2013, **15**, 5168–5178.
37 P. Khakhlary, C. E. Anson, A. Mondal, A. K. Powell and J. B. Baruah, *Dalton Trans.*, 2015, **44**, 2964–2969.
38 *Rigaku OD, CrysAlis PRO*, Rigaku Oxford Diffraction Ltd, Yarnton, England, 2015.
39 G. M. Sheldrick, *Acta Crystallogr., Sect. C: Struct. Chem.*, 2015, **71**, 3.
40 O. V. Dolomanov, L. J. Bourhis, R. J. Gildea, J. A. K. Howard and H. J. Puschmann, *Appl. Crystallogr.*, 2009, **42**, 339.
41 P. McArdle, P. Daly and D. Cunningham, *J. Appl. Crystallogr.*, 2002, **35**, 378.
42 A. L. Spek, *Acta Crystallogr., Sect. C: Struct. Chem.*, 2015, **71**, 9–18.

